Coronal Plane Spine Twisting Composes Shape To Adjust the Energy Landscape for Grounded Reorientation

J. Diego Caporale[†], Benjamin W. McInroe[⋆], Chenze Ning[†], Thomas Libby[*], Robert J. Full[§], Daniel E. Koditschek[‡]

***Abstract*— Despite substantial evidence for the crucial role played by an active backbone or spine in animal locomotion, its adoption in legged robots remains limited because the added mechanical complexity and resulting dynamical challenges pose daunting obstacles to characterizing even a partial range of potential performance benefits. This paper takes a next step toward such a characterization by exploring the quasistatic terrestrial self-righting mechanics of a model system with coronal plane spine twisting (CPST). Reduction from a full 3D kinematic model of CPST to a two parameter, two degree of freedom coronal plane representation of body shape affordance predicts a substantial benefit to ground righting by lowering the barrier between stable potential energy basins. The reduced model predicts the most advantageous twist angle for several cross-sectional geometries, reducing the required righting torque by up to an order of magnitude depending on constituent shapes. Experiments with a three actuated degree of freedom physical mechanism corroborate the kinematic model predictions using two different quasistatic reorientation maneuvers for both elliptical and rectangular shaped bodies with a range of eccentricities or aspect ratios. More speculative experiments make intuitive use of the kinematic model in a highly dynamic maneuver to suggest still greater benefits of CPST achievable by coordinating kinetic as well as potential energy, for example as in a future multi-appendage system interacting with a contact-rich 3D environment.**

I. INTRODUCTION

Biological backbones or spines provide numerous locomotor benefits to vertebrates. They enable dynamic gaits such as galloping and bounding [1], [2], reorientation maneuvers such as zero net angular momentum righting [3], [4], and can serve to increase the workspaces of the limbs for interaction. Analogously, dynamic, multi-degree of freedom robotic spines are poised to enable a myriad of new capabilities for legged robots [5], [6], [7], [8]. However, the adoption of spines in existing dynamic legged robots remains limited, in part because they introduce complicated dynamics that must be controlled, and their full range of potential locomotor benefits has not yet been characterized. Towards a thorough analysis of the dynamics of spined systems in contact rich environments, we take the first step by exploring the quasistatic terrestrial self-righting mechanics of a model spine system with coronal plane spine twisting (CPST), a degree of freedom that remains relatively uncommon in existing robot spine morphologies.

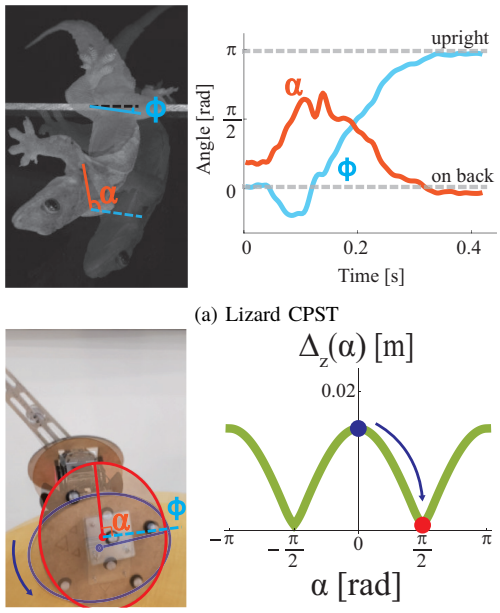

Fig. 1: (a) (left) A lizard demonstrating CPST while performing a self-righting maneuver. ϕ is the roll angle of the hips, and α is the relative angle between shoulders and hips in the roll axis. (right) α and ϕ traces during the righting maneuver. (b) (left) TPM performing a self-righting maneuver using CPST. (right) Quasistatic prediction of potential energy barrier reduction by CPST as explained in Eq. 12.

A locomotor's ability to recover or reorient itself following inevitable slips and falls in unpredictable or inimical environments depends critically on its morphology, inertial parameters, and actuator characteristics in a manner that can be captured using the concept of energy landscapes [9], [10], [11]. This understanding calls particular attention to the importance of overcoming energy barriers in both animals and machines [12], [13]. Algorithms exploiting single degree of freedom shape change such as zero net angular momentum reorientation for aerial righting have drawn inspiration from falling cats [14], [15] and lizards [16], [17], employing robotic spines and tails respectively. Strategies for ground righting have included the use of contact [9], inertial [18] and gravitational moments [9], but most have been embodied in robot morphologies via specific appendages such as

[†] Mechanical Engineering and Applied Mechanics, University of Pennsylvania, PA, USA. {jdcap,ningcz}@seas.upenn.edu
[⋆] Biophysics Graduate Group, University of California, Berkeley, CA, USA. bmcinroe@berkeley.edu
[*] SRI International, Menlo Park, CA, USA. tom.libby@sri.com
[§] Department of Integrative Biology, University of California, Berkeley, CA, USA. rjfull@berkeley.edu
[‡] Electrical and Systems Engineering, University of Pennsylvania, PA, USA. kod@seas.upenn.edu
This work was supported in part by the US Army Research Office under grant W911NF-17-1-0229.

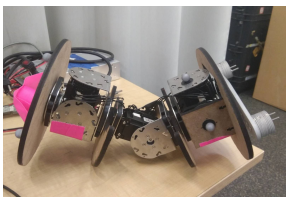

(a) Torso Physical Model (TPM)

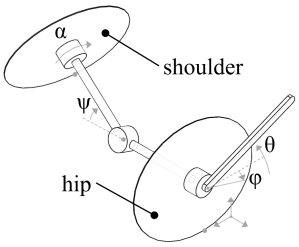

(b) Robot Schematic

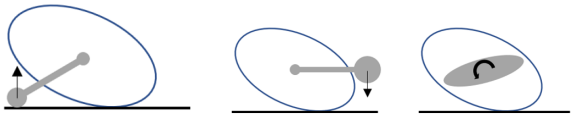

(c) Reorientation Strategies

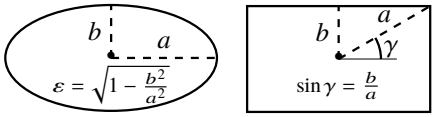

(d) Shape Parameters

Fig. 2: (a) The TPM is made up of CKBot modules[23], a tail, and MDF plates. (b) TPM's kinematic model. This system can offset the angle of the "shoulder" with respect to the "hips" to affect the potential energy of the system. The two lamina are identical convex shapes that are not necessarily elliptical. In this study, the sagittal bending, ψ in (c), is used to reset α between trials and is not yet used to assist the reorientation. (c) The different modes of tail powered reorientation. (d) A description of the relevant shape parameters.

tails [19], wings [12], and limbs [20]. In hyper-redundant serpenoid and modular robots, active shape control has been employed to affect stability for rolling maneuvers [21], [22], [23].

A. Contributions and Organization

This paper explores the hypothesis that coronal plane spine twisting (CPST), a degree of freedom observed in ground righting lizards (Fig 1.a) [24], can be used to reduce the effort of grounded reorientation in robots. In Sec. II, we derive the kinematics of a 3D spatial model for a body with a twisted torso in rolling contact with the ground, showing that the changes of internal body shape and contact configuration resulting from varying the torso twist affect the 3D rolling kinematics of the CoM. A succession of simplifying approximations allows kinematic reduction of the 6 DoF spatial model to a simple 2 DoF planar model described by a shape parameter and the spinal "twist" parameter, α. We use this model to show that CPST can substantially reduce the quasistatic potential energy barrier for rolling.

In Sec. III, we challenge the utility of this highly simplified analysis for real physical mechanisms by introducing the torso physical model, TPM, a bioinspired 3 actuated DoF tailed and spined system with an adjustable pair of laminar

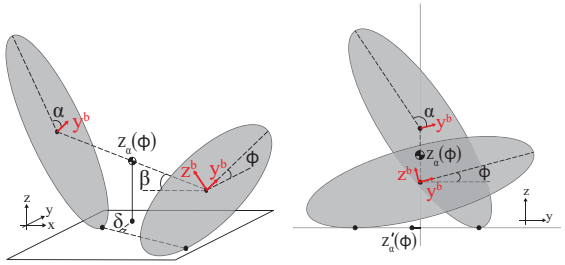

(a) Spatial Model (b) Coronal Plane Reduction

Fig. 3: A kinematic model in 3-space (a) and the reduced order model in the coronal plane (b). Note that a small pitch would be induced by the phase offset, α, but, as shown in Section II-B.2, it can be ignored by assuming $\beta \approx 0$. For any given shapes, $z_\alpha(\phi)$ is equal to the average COM height of both shapes and $z'_\alpha(\phi)$ gives an approximation of δ, the effective contact point offset (also shown in Section II-B.2). This model allows us to predict the effect of Coronal Plane Spine Twisting (CPST) on energetic and torque requirements.

shapes[1] to model the cross-sectional profile of a legged robot. We perform experiments measuring the minimum torque necessary to right using two distinct tail righting actuation strategies, contact and shape change righting, for model bodies with elliptic and rectangular cross sections of a range of eccentricities and aspect ratios. Our results demonstrate a torque reduction factor between 1.5 and 8.7 for the optimal choice of body twist angle, $\alpha = \alpha^*$, dependent on body cross-sectional shape. We further show that the reduced coronal plane model accurately predicts α^* for all body shapes and twist angles tested using the fully 3D TPM. We then present preliminary empirical results demonstrating the benefits of CPST for a dynamic inertial appendage driven righting maneuver.

In Sec. IV, we summarize our theoretical and empirical findings on the general benefits of CPST for ground righting, and discuss plans for future work employing actuated spines for dynamic terrestrial reorientation maneuvers.

II. Quasistatic Modeling of CPST

Aiming eventually (beyond the scope of this paper) for a low degree of freedom CPST dynamical template [25] that might be effectively anchored in both animal data (Fig. 1.a) and robot controllers (e.g. as suggested in Fig. 2c), this section presents a reduction from a notional pair of twisting, tilted, shaped spatial plates to a two parameter, 2 DoF kinematic model as follows. After a brief review of rudimentary "roulette theory" [26], [27] in Sec. II-A, the lamina (Fig. 3a) are projected onto their conjoined coronal planes (Fig. 3b) in Sec. II-B and the composition of their effective shape reveals the potential benefit of a coronal plane twist as determined by laminar shape in Sec. II-C. Fig. 4 summarizes the influence on the resulting 2 DoF effective rolling planar shape of the two composition parameters, twist, α, and shape — captured by either the eccentricity, ϵ, of an ellipse or the aspect ratio, γ, of a rectangle — as depicted in Fig. 2d.

[1]Laminar shape here refers to a planar body whose contour is described by a contour C.

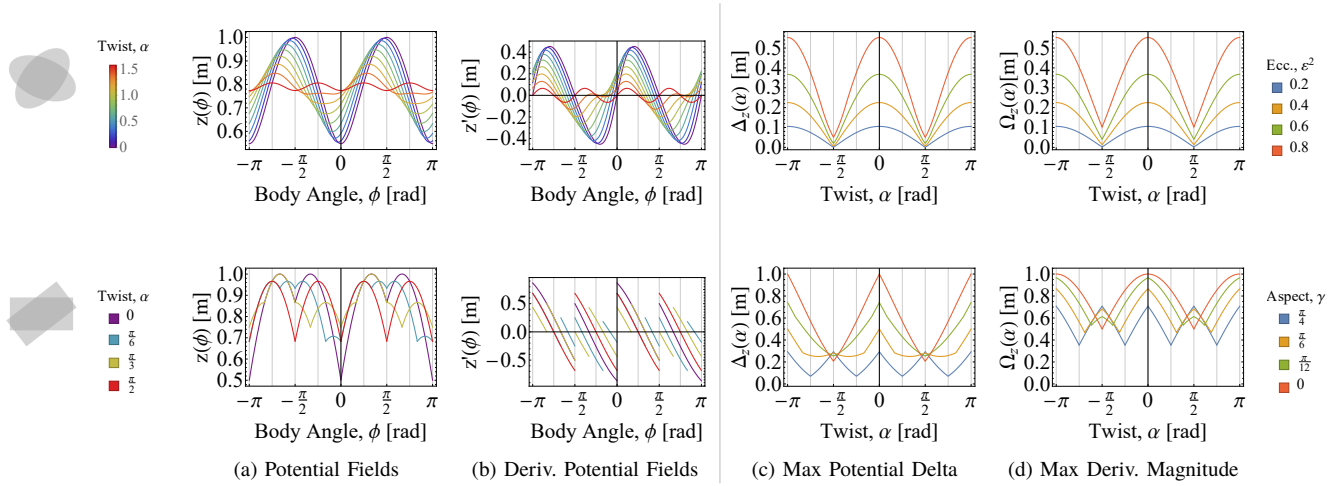

(a) Potential Fields (b) Deriv. Potential Fields (c) Max Potential Delta (d) Max Deriv. Magnitude

Fig. 4: Investigating the effective shape and potential energy functions of two two-lamina systems: elliptical plates (top) and rectangular plates (bottom). The effect of CPST (parameterized by α) on (a) the COM height and (b) the derivative of the COM height for a given ellipse ($\epsilon^2 = .8$) and rectangle ($\gamma = \pi/6$, the angle of the diagonal to horizontal). CPST has a large effect on both the potential energy barrier and the torque (proportional to the derivative) necessary to reorient, even when accounting for the discontinuity of the rectangle. (c) The difference between the minimum and maximum potential energy for several different eccentricities (top) and aspect ratios (bottom) as a function of α, (see Eq.12). (d) The largest magnitude derivatives for several eccentricities as a function of α, (see Eq. 13). In the elliptical example the most beneficial CPST angle α is constant regardless of eccentricity at $\pi/2$. Unlike the elliptical example, the most beneficial α is not constant with respect to γ in either the quasistatic or dynamic sense, with the optimal α's moving continuously from $\pi/2$ to $\pi/4$ for γ's from 0 to $\pi/4$. Note: $\gamma = \pi/4$ is a square and therefore every rectangle is described by $\gamma \in [0, \pi/4]$.

Two key approximations in Sec. II-B.2 underlie these reductions. First, we assume that the two lamina lie in parallel vertical planes. Second, we presume an "elongated body" (rendered formally by asserting $l >> d_\alpha(\phi)$ in Eq. 6) to simplify the expression of the moment arm of the mass center on the coronal plane center of rotation. While the second surely applies to some bodies, the first is in tension with the very effect of interest — the discrepancy in the laminar shapes' mass center heights when one is rotated relative to another. The experiments presented in Sec. III relieve the worry that the appealing simplicity of this composed model is achieved at too great an expense of accuracy.

A. *Kinematics of Planar Rolling Bodies*

We describe the kinematics and dynamics of a planar body, parameterized as a closed curve C, rolling in the yz-plane (referring throughout this discussion to the spatial world frame depicted in Fig. 3a) without slip on the horizontal (y-axis) using the trajectory of the shape's center of mass (COM) and the COM's relation to the point of contact with the ground.

Specifically, the trajectory of the COM is a *roulette* (a curve created by following a point fixed to rolling shape) and can be parameterized as $\mathbf{x}_{COM}(\theta) = [\chi(\theta), \sigma(\theta)]^T$, where θ describes the angle of rotation of the shape with respect to the horizontal [26], [27].[2] In this work, we focus on a quasistatic analysis of shapes with mass rolling in the plane due to external torques; horizontal translation ($\chi(\theta)$) has no effect on the net forces and moments (since the system is only affected by gravitational potential energy) and so can be ignored and we will describe the COM purely by its height, ($\sigma(\theta)$).

[2] By the roulette lemma [26] [27], $\sigma(\theta) = \chi'(\theta)$.

Although the absolute horizontal position does not figure in this analysis, horizontal offset from the COM of the contact point is needed to calculate gravitational torque, and this can be obtained as follows from a nice result about ellipses[28]. Namely, an ellipse (Fig. 2d) with eccentricity ε, semi-major axis a, and fixed frame at its center has a contact point parameterized as $CP = [\,-\sigma'(\theta)\ -\sigma(\theta)\,]^T$ where

$$\sigma(\theta) = \sigma_e(\theta) = a\sqrt{1 - \epsilon^2 \cos\theta}. \tag{1}$$

A similar derivation of ellipse kinematics is seen in [21]. Furthermore, a frame of reference directly below the ellipse's center on the y-axis is chosen, such that the contact point and the COM are

$$\mathbf{x}_{CP} = \begin{bmatrix} -\sigma'(\theta) \\ 0 \end{bmatrix} \qquad \mathbf{x}_{COM} = \begin{bmatrix} 0 \\ \sigma(\theta) \end{bmatrix}. \tag{2}$$

The same relationship between the COM and contact point would hold for any convex polygons (or the convex hull of any polygon), though $\sigma_p(\theta)$ is only piecewise differentiable because of the flat sides and $\sigma_p'(\theta)$ would be discontinuous[3]. For example, a rectangle with semi diagonal length a and diagonal angle from the horizontal γ (Fig. 2d) can be described with

$$\sigma_r(\theta) = a \sin\left((-1)^{\left\lfloor \frac{2\phi}{\pi} \right\rfloor}\gamma + (\phi \bmod \pi)\right) \tag{3}$$

$$\sigma_r'(\theta) = a \cos\left((-1)^{\left\lfloor \frac{2\phi}{\pi} \right\rfloor}\gamma + (\phi \bmod \pi)\right). \tag{4}$$

[3] Polygons act as elliptical shapes of eccentricity $\varepsilon = 1$, i.e. setting the semi-minor axis $b = 0$, like a set of rotating bars switching at defined angles akin to the rimless wheel. Using this elliptical analogy allows us to take advantage of the derivative relationship from [28] albeit carefully avoiding dividing by zero.

B. Two Lamina Torso Model

Starting with the rolling bodies described in the previous section, we create a system with two lamina[4] fixed to one other by a revolute joint. We seek to further understand this spatial model's kinematics (Section II-B.1) as well as reduce it to a planar model (Section II-B.2).

1) Spatial: As depicted in Fig. 3(a), the model consists of two identical shapes (ellipses in the figure) attached at the centers by a perpendicular bar of length l. Between them we attach a revolute joint to act as a spine and allow for CPST of angle α. We define one of the ellipses as the "hips" of our system and measure the body angle, ϕ, with respect to the horizontal. This system is non-holonomic, and rolling over from external force/torque or changing α induces pitching and yawing due to the no-slip constraints. Since this analysis is static, the coordinate system can be placed at the projection of the center of the "hips" on the ground, with z-axis vertical and x-axis the projection of the connecting bar, similarly to the single planar body analysis. Essentially, we can ignore the yaw and travel in the plane of the system, therefore ignoring the non-holonomic effects.

The system CoM position is then

$$\mathbf{x}_{COM} = \begin{bmatrix} \frac{l}{2}\cos\beta \\ 0 \\ \frac{1}{2}\cos\beta\,(\sigma(\phi)+\sigma(\phi+\alpha)) \end{bmatrix} \tag{5}$$

In an effort to be analogous to the analysis of Section II-A and to facilitate model reduction, we define an effective system contact point as the distance, δ, from the COM projected on the floor to the contact line defined by the hip and shoulder contact points, which can be written

$$\delta = \frac{l s'_\alpha(\phi)\cos(\beta) + 2\sin(\beta)\, g_\alpha(\phi)}{2\sqrt{(l\cos(\beta) - d_\alpha(\phi)\sin(\beta))^2 + d'_\alpha(\phi)^2}}. \tag{6}$$

with

$$\begin{aligned} d_\alpha(\phi) &= (\sigma(\phi) - \sigma(\phi+\alpha)) \\ s_\alpha(\phi) &= (\sigma(\phi) + \sigma(\phi+\alpha)) \\ g_\alpha(\phi) &= (\sigma(\alpha+\phi)\,\sigma'(\phi) - \sigma(\phi)\,\sigma'(\alpha+\phi)\,) \\ \beta_\alpha(\phi) &= \arctan 2(d_\alpha(\phi), l) \end{aligned}$$

Removing β with trig identities we obtain

$$\delta = \frac{l^2 s'_\alpha(\phi) + 2 d_\alpha(\phi)\,(\sigma'(\phi)\,\sigma(\alpha+\phi) - \sigma'(\alpha+\phi)\,\sigma(\phi))}{2\sqrt{\left(l^2 - d_\alpha(\phi)^2\right)^2 + (l^2 + d_\alpha(\phi)^2)\, d'_\alpha(\phi)^2}}. \tag{7}$$

We will now derive an approximate planar reduction to simplify analysis and serve as a starting point for a future dynamical template.

2) Coronal Plane Reduction: We now analyze the system on the coronal plane. Assuming $\beta \approx 0$, which is the case when $l >> d_\alpha(\phi)$, we reduce $\mathbf{x}_{COM}$ to

$$z_\alpha(\phi) = \frac{(\sigma(\phi) + \sigma(\phi+\alpha))}{2}. \tag{8}$$

[4]See footnote 1.

Following the results from [28] for a single shape, we would be tempted to set the contact point to $z'_\alpha(\phi)$, and use this relationship to describe an effective shape, instead we attempt to understand its relationship to δ. Furthermore, we reduce δ using Eq. 6 and small β such that,

$$\delta|_{\beta=0} = \frac{l s'_\alpha(\phi)}{2\sqrt{l^2 + d'_\alpha(\phi)^2}}.$$

We must make one more approximation in δ that $l >> d'_\alpha(\phi)$, which again for many shapes follows from the first assumption. Note also that when $d'_\alpha(\phi)$ is large (in magnitude) $s'_\alpha(\phi)$ is small and vice versa. And so, we assume

$$\begin{aligned} \beta \approx 0, \quad & \frac{l}{\sqrt{l^2 + d'_\alpha(\phi)^2}} \approx 1 \\ \implies \delta &\approx \frac{s'_\alpha(\phi)}{2} = z'_\alpha(\phi). \end{aligned}$$

C. Potential Energy Benefits of CPST

Having shown that the COM and the contact point of the rolling composite shape can be approximated as averaged functions of its two constituents[5], we call attention to the following observation. First, notice that C is a closed curve hence the functions $\sigma(\phi)$ and $\sigma'(\phi)$ are bounded. Next, notice that given any bounded periodic function $f : \mathbb{S}^1 \to \mathbb{R}$ with $b_l \le f(\theta) \le b_u$, a weighted average of phase shifted instances

$$\bar{f}(\theta; c_1, c_2, ..., c_n) \equiv \frac{\sum_{i=1}^n \alpha_i f(\theta + c_i)}{\sum_{i=1}^n \alpha_i} \tag{9}$$

preserves those bounds, i.e. $b_l \le \bar{f}(\theta; c_1, ..., c_n) \le b_u$.

It follows that

$$z_\alpha(\phi) \le \sigma(\phi) \tag{10}$$

$$z'_\alpha(\phi) \le \sigma'(\phi) \tag{11}$$

for all α. Since the system (before adding actuated torques) only has gravity acting on it, we can take the COM height, $z_\alpha(\phi)$, as an analog (scaled) to potential energy and similarly, its derivative, $z'_\alpha(\phi)$ as an analog for the torque produced by gravity (the lever arm associated with gravity). Thus, by Eqs. 10 and 11, a twist in the body via CPST can only benefit the reorientation task (a roll from $\phi = 0 \to \pi$).

Further we define,

$$\Delta_z(\alpha) \equiv \sup_\phi \{z_\alpha(\phi)\} - \inf_\phi \{z_\alpha(\phi)\} \tag{12}$$

$$\Omega_z(\alpha) \equiv \sup_\phi \left\{\left|z'_\alpha(\phi)\right|\right\} \tag{13}$$

as a useful heuristic for potential boundary and a direct analog to minimum required torque to reorient quasistatically, respectively. Figs. 4 (a) and (b) show the effect on potential energy and torque, respectively, for an ellipse and a rectangle, noting that when $\alpha = 0$ this model is equivalent to the single shape in the plane. Furthermore, in (c) and (d), we show that we can choose α to give the best benefits either energetically

[5]This would still be true if it was instead a weighted averages with different massed shapes, but the benefit would be smaller.

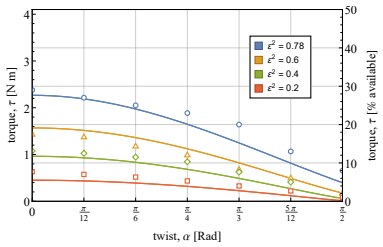

(a) Elliptical Plate system

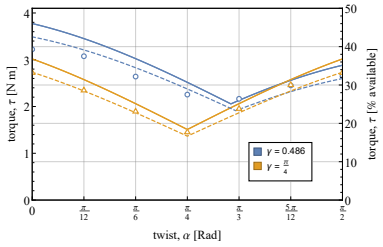

(b) Rectangular Plate System

Fig. 5: Contact righting experimental data using the TPM and employing CPST. The expected torque (solid lines), τ_α, described in Section III-B, matches the measured torque input, τ_c, (points) across all runs. (a) Investigating CPST for the ellipses with eccentricities ε. (b) Similarly, two rectangles with aspect angles γ were tested. The robot has rounded corners (radius 1 cm) and the required torque for this model (dashed) is better. Each plot manifests a visually apparent α^* at which the torque is minimized, matching with the pure analysis shown in Fig. 4.

or quasistatically, by comparing the difference of the potential energy bounds, $\Delta_z(\alpha)$ and maximum magnitude of the torque necessary to flip $\Omega_z(\alpha)$.

We could do this for any shape, though the structure presented by an ellipse and a rectangle make it easier to present the benefits. Note that for an ellipse the eccentricity plays no role in choosing the optimal α at $\pi/2$, but for a rectangle the optimal α ranges from $\pi/2$ for a thin bar to $\pi/4$ for a square.

III. Experiments

A. Robot Design

The TPM, seen in Fig. 2a, is a simple robot meant to act as a physical model for CPST assisted reorientation. The system consists of three CKBots [23] in the configuration shown in Fig. 2 along with four MDF, laser cut plates, a tail, and counterweights (to keep the COM centered after the addition of a massive tail). The two inner plates are used to support the robot during sagittal spine bending. Sagittal bending is only used to facilitate twisting before reorienting– and is always locked during experiments reported here – but could be used in the future to support more complex maneuvers. Recall, the CPST angle, α, remains constant during the righting maneuver only changing before the maneuver and after the hips reach the goal state ($\phi = \pi$). The CKBots are built around Dynamixel EX-106+ motors, which (at 15V) have a holding torque of 8.2 N-m and a no load speed of 54.9 RPM. For the TPM, the torque on these motors is never the limiting factor for reorientation (given their high gearing)

TABLE I: Experimental results for contact righting with CPST. Using data from Fig. 5, we find the best α for reorientation, designated α^*. By directly comparing best and worst case torques, $\tau|_{\alpha=\alpha^*}$ and $\tau|_{\alpha=0}$ resp., we see there is a significant benefit to using CPST, especially to the elliptical bodies where we reduce the necessary torque by a factor of between 3 and 9 while the rectangles benefit by a factor of between 1.5 and 2.

	Ellipses, ε^2				Rectangles, γ	
	0.2	0.4	0.6	0.8	0.49	$\pi/4$
Optimal CPST, α^*	$\pi/2$	$\pi/2$	$\pi/2$	$\pi/2$	$\pi/3$	$\pi/4$
$\tau\|_{\alpha=0}$ [N-m]	0.63	1.07	1.43	2.38	3.22	2.72
$\tau\|_{\alpha=\alpha^*}$ [N-m]	0.08	0.15	0.16	0.66	2.16	1.45
Torque Reduction	87%	86%	89%	72%	33%	47%
Meas. Redu. Factor	7.7	7.3	8.7	3.6	1.5	1.9

but we will discover limitations created by their speed and the physical parameters of the different self righting strategies (Fig. 2c).[6]

TABLE II: Nominal Robot Parameters

Mass w.o. Tail	2.5 kg
Tail Mass (varies by experiment)	$\approx$ 0.4 kg
Body Length (unbent), l	0.3 m
Tail Length	0.3 m
Max Shape Radius, a	0.15 m

B. Realizing Tail Contact

Because contact righting (Fig. 2c) allows us to take (almost) full advantage of the system's torque capabilities, this method is best suited for testing the model and the cases where the assumptions may fail. Because this method works quasistatically, we look to apply the minimum torque which allows the body to right for a variety of values of α and body shapes, similarly to the methods of [21]. Eq. 13 details our expected minimum torque up to a constant, in particular $\tau_\alpha \equiv mg\Omega_z(\alpha)$, where m is the total mass of the robot (2.8 kg) and g is gravitational acceleration (9.81 m/s).

We used a variety of elliptical and rectangular girdle pieces and performed a manual search for a decision surface between success ($\phi \to \pi$) and failure. In Fig. 5, we see that the measured decision surface matches the predicted surface well, and therefore that the reduced model captures the necessary minimum torque to right, allowing us to predict optimal values of α for the tested shapes.

We note two practical considerations from these experiments. The reported torques have the intrinsic motor friction torque subtracted, which was measured by finding the minimum torque for which the tail rotated without load. For the rectangle with $\gamma = 0.486$, we increased the tail length to 0.6 m, as the 0.3 m tail induced a large vertical contact force that caused the hip segment to break contact with the ground, an effect that we do not explore but consider for future work.

It should be noted that the robot fails to meet the long length and small eccentricity assumptions we laid out in our analysis, but the approximations are sufficiently robust that

[6] To control the joints, we send torque commands to the tail and shoulder continuously rotating joints and position commands to the bending joint. The torque commands are sent as percentages of the max torque.

TABLE III: Gravitational Shape Change Tests. As expected, the capabilities of the tail are limited by its max torque available, τ_{pred}, defined in Section III-C. Asterisks indicate configurations that could not be flipped quasistatically with just shape change righting. Namely, we succeed across all these configurations with $\alpha = \pi/2$, and we expect that we can use the CPST to reduce tail mass and/or length at design time. To verify our results, τ_{max} is the measured max torque over which the tail begins free rotating and should be about equal to τ_{pred}. The torques required to right using shape change, τ_{sc}, are close to the torques required to right using contact, τ_c (as in Fig. 5). All torques in N-m.

CPST	Shape Change			Contact	
α	Torque Results, τ_{sc}			Torque, τ_c	
0	*	*	*	1.59	1.07
15	*	1.05	*	1.53	1.03
30	*	0.93	*	1.34	0.94
45	*	0.86	*	1.15	0.84
60	1.05	0.64	0.55	0.84	0.62
75	0.74	0.40	0.39	0.66	0.41
90	0.42	0.21	0.23	0.33	0.15
ε^2	0.6	0.4	0.4†	0.6	0.4
τ_{pred}	1.28	1.28	0.94	-	-
τ_{max}	1.08	1.08	0.70	-	-

† Trial uses same eccentricity but different tail.

we see agreement between the predictions and empirical data for even the highest aspect ratio rectangle ($\gamma = 0.486$) and ellipse ($\varepsilon^2 = .78$) with a pitch of about 15 degrees in both cases. As such, we strongly suspect that the torque reduction benefits of CPST for ground righting and the predictive power of our model generalize to many robot body shapes.

C. Shape Change

Unlike the contact righting strategy which is limited by actuator torque, shape change righting is inherently limited by the body morphology. Given a tail with mass m_t and distance d_t between the center of mass of the tail and its center of rotation, the maximum torque expected due to gravity is $\tau_{pred} = m_t g d_t$. Any further torque supplied to the tail will lift the tail past the horizontal and cause it to continuously rotate, a failure case in these tests.

Test were run by slowly ramping up the torque input until the robot either reoriented (success, at which point the torque, τ_{sc} is recorded) or the tail began to rotate freely (failure, at which point the max torque was measured, τ_{meas}). The torque required to self-right should be approximately equal to the previous contact righting test with discrepancies caused by the added tail weight. In Table III, we show three different robot configurations, with two different eccentricities and two different tails. The tails are characterized by their τ_{pred}.[7] We observe the same trends in Table III seen in Fig. 5. These results suggest a further benefit of our model as being agnostic to torque input type or strategy.

CPST's torque benefit allows a user hoping to achieve a shape change righting behavior to significantly reduce the mass and/or length of a tail (or other weighted appendage) at design time.

[7]It should be noted that tails still need to have masses much smaller than the body of the robot or the COM will shift toward the back of the robot, requiring a mass-weighted average for our approximation of $z_\alpha(\phi)$

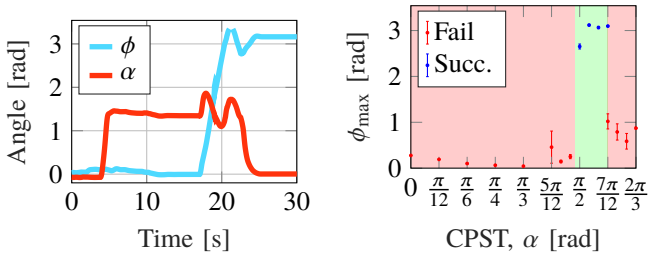

(a) Inertial Righting Example (b) CPST Success

Fig. 6: Inertial Reorientation Righting Experiment. For a modest eccentricity with a modest tail inertia, CPST allows the system to flip where it would otherwise fail. In this test, the tail actuator was given max torque command for every trial. The speed limitations of the CKBots enforce a maximum energy input of 0.28 J (calculated from the tail inertia ($\approx$ .014 kg m^2) and rotation rate from vicon ($\approx$ 1 rev/s)). Our analysis suggest the energy barrier for reorientation is 0.04 J at $\alpha = \pi/2$ (vs 2.8 J at $\alpha = 0$), which matches with the findings in (b), where ϕmax is the nearest to the goal state the robot made it before oscillating.

D. Towards Inertial Reorientation

Our analysis so far has been purely kinematic and quasistatic, but we empirically explored an inertial reorientation method as well. Using a symmetric tail to minimize configuration-dependent gravitational torques set to maximum torque input, we hang the tail over the edge of our working surface to allow free rotation without tail contact. As mentioned in Section III-A, the CKBots are severely speed limited and so our max angular impulse is similarly limited (discounting the uninteresting recourse to heavier tails, which, in any case, require more counter weight and make the robot harder to right). Nevertheless, we found that the elliptical robot could successfully reorient in a small neighborhood of $\alpha = \pi/2$ (Fig. 6b), having struggled to right with other CPST angles (again, rejecting aggressively increased tail weight and inertia). This suggests that there is also an energetic benefit to the CPST maneuver, as is implied by our analysis in Fig. 4a and Eq. 12, encouraging us to move toward a dynamic analysis of this system, directly tuning the potential landscape.

IV. CONCLUSIONS

Our findings demonstrate the utility of CPST for quasistatic ground righting behaviors by reducing the torque necessary for reorientation. Measurements of the minimum torque necessary to right for the quasi-static maneuvers (depicted in first two sketches of Fig. 2c) using both tail ground contact (Fig. 5) and tail shape change primitives (Table III) show close agreement with the theoretical torque reduction predictions of Sec. II (Table I). We further explore a more speculative third strategy, inertial self righting (rightmost sketch of Fig 2c), not yet addressed by our quasistatic analysis, but which nonetheless suggests promising results.

Future work will explore the integration of CPST with dynamic appendage actuation, and the role of relative phasing between spine and tail actuation during righting. The reduced planar model of CPST derived in Sec. II-B.2 provides a first step towards a dynamical template for ground righting with an actuated spine.

References

[1] R. M. Alexander, N. J. Dimery, and R. Ker, "Elastic structures in the back and their role in galloping in some mammals," *Journal of zoology*, vol. 207, no. 4, pp. 467–482, 1985.

[2] N. Schilling and R. Hackert, "Sagittal spine movements of small therian mammals during asymmetrical gaits," *Journal of Experimental Biology*, vol. 209, no. 19, pp. 3925–3939, 2006.

[3] T. Kane and M. Scher, "A dynamical explanation of the falling cat phenomenon," *International Journal of Solids and Structures*, vol. 5, no. 7, pp. 663–670, 1969.

[4] A. Jusufi, D. I. Goldman, S. Revzen, and R. J. Full, "Active tails enhance arboreal acrobatics in geckos," *Proceedings of the National Academy of Sciences*, vol. 105, no. 11, pp. 4215–4219, 2008.

[5] G. A. Folkertsma, S. Kim, and S. Stramigioli, "Parallel stiffness in a bounding quadruped with flexible spine," in *2012 IEEE/RSJ International Conference on Intelligent Robots and Systems*. IEEE, 2012, pp. 2210–2215.

[6] S. Seok, A. Wang, M. Y. M. Chuah, D. J. Hyun, J. Lee, D. M. Otten, J. H. Lang, and S. Kim, "Design principles for energy-efficient legged locomotion and implementation on the mit cheetah robot," *Ieee/asme transactions on mechatronics*, vol. 20, no. 3, pp. 1117–1129, 2014.

[7] M. Khoramshahi, A. Spröwitz, A. Tuleu, M. N. Ahmadabadi, and A. J. Ijspeert, "Benefits of an active spine supported bounding locomotion with a small compliant quadruped robot," in *2013 IEEE International Conference on Robotics and Automation*. IEEE, 2013, pp. 3329–3334.

[8] J. Duperret, B. Kramer, and D. E. Koditschek, "Core actuation promotes self-manipulability on a direct-drive quadrupedal robot," in *International Symposium on Experimental Robotics*. Springer, 2016, pp. 147–159.

[9] C. C. Kessens, D. C. Smith, and P. R. Osteen, "A framework for autonomous self-righting of a generic robot on sloped planar surfaces," in *2012 IEEE International Conference on Robotics and Automation*. IEEE, 2012, pp. 4724–4729.

[10] C. Li, A. O. Pullin, D. W. Haldane, H. K. Lam, R. S. Fearing, and R. J. Full, "Terradynamically streamlined shapes in animals and robots enhance traversability through densely cluttered terrain," *Bioinspiration & biomimetics*, vol. 10, no. 4, p. 046003, 2015.

[11] D. J. Kriegman, "Let them fall where they may: Capture regions of curved objects and polyhedra," *The International Journal of Robotics Research*, vol. 16, no. 4, pp. 448–472, 1997.

[12] C. Li, C. C. Kessens, R. S. Fearing, and R. J. Full, "Mechanical principles of dynamic terrestrial self-righting using wings," *Advanced Robotics*, vol. 31, no. 17, pp. 881–900, 2017.

[13] C. Li, T. Wöhrl, H. K. Lam, and R. J. Full, "Cockroaches use diverse strategies to self-right on the ground," *Journal of Experimental Biology*, vol. 222, no. 15, p. jeb186080, 2019.

[14] K. Yamafuji, T. Kobayashi, and T. Kawamura, "Elucidation of twisting motion of a falling cat and its realization by a robot," *Journal of the Robotics Society of Japan*, vol. 10, no. 5, pp. 648–654, 1992.

[15] J. Zhao, L. Li, and B. Feng, "Effect of swing legs on turning motion of a free-falling cat robot," in *2017 IEEE International Conference on Mechatronics and Automation (ICMA)*. IEEE, 2017, pp. 658–664.

[16] A. Jusufi, D. T. Kawano, T. Libby, and R. J. Full, "Righting and turning in mid-air using appendage inertia: reptile tails, analytical models and bio-inspired robots," *Bioinspiration & biomimetics*, vol. 5, no. 4, p. 045001, 2010.

[17] E. Chang-Siu, T. Libby, M. Brown, R. J. Full, and M. Tomizuka, "A nonlinear feedback controller for aerial self-righting by a tailed robot," in *2013 IEEE International Conference on Robotics and Automation*. IEEE, 2013, pp. 32–39.

[18] C. C. Kessens and J. Dotterweich, "Ground-based self-righting using inertial appendage methods," in *Unmanned Systems Technology XIX*, vol. 10195. International Society for Optics and Photonics, 2017, p. 1019505.

[19] C. S. Casarez and R. S. Fearing, "Dynamic terrestrial self-righting with a minimal tail," in *2017 IEEE/RSJ International Conference on Intelligent Robots and Systems (IROS)*. IEEE, 2017, pp. 314–321.

[20] J. Hwangbo, J. Lee, A. Dosovitskiy, D. Bellicoso, V. Tsounis, V. Koltun, and M. Hutter, "Learning agile and dynamic motor skills for legged robots," *Science Robotics*, vol. 4, no. 26, p. eaau5872, 2019.

[21] R. L. Hatton and H. Choset, "Sidewinding on slopes," in *2010 IEEE International Conference on Robotics and Automation*. IEEE, 2010, pp. 691–696.

[22] C. Gong, R. L. Hatton, and H. Choset, "Conical sidewinding," in *2012 IEEE International Conference on Robotics and Automation*. IEEE, 2012, pp. 4222–4227.

[23] J. Sastra, S. Chitta, and M. Yim, "Dynamic rolling for a modular loop robot," *The International Journal of Robotics Research*, vol. 28, no. 6, pp. 758–773, 2009.

[24] B. McInroe, T. Libby, D. Koditschek, and R. Full, "Identifying control modules in complex, dynamic behaviors by using ground-righting in geckos," in *Integrative and Comparative Biology*, vol. 59. Oxford Univ Press INC Journal Dept, 2001 Evans RD, Cary, NC 27513 USA, 2019, pp. E154–E154.

[25] R. J. Full and D. E. Koditschek, "Templates and anchors: neuromechanical hypotheses of legged locomotion on land," *Journal of experimental biology*, vol. 202, no. 23, pp. 3325–3332, 1999.

[26] F. Kuczmarski, "Roads and wheels, roulettes and pedals," *The American Mathematical Monthly*, vol. 118, no. 6, pp. 479–496, 2011.

[27] U. Abel, L. Beukemann, and V. Kushnirevych, "Rolling curves: An old proof of the roulette lemma," *The American Mathematical Monthly*, vol. 124, no. 8, pp. 723–736, 2017.

[28] R. Rostamian, "The dynamics of an ellipse rolling without slipping on a horizontal line within a vertical plane," *Unpublished*, Apr. 2019. [Online]. Available: https://www.mapleprimes.com/DocumentFiles/210428_post/rolling-ellipse.pdf